Nanoscale

ARTICLE

Au@Ag SERRS tags coupled to a lateral flow immunoassay for the sensitive detection of Pneumolysin

Received 00th January 20xx,
Accepted 00th January 20xx

DOI: 10.1039/x0xx00000x

www.rsc.org/

Lucía Blanco-Covián,[a] Verónica Montes-García,[b] Alexandre Girard,[c] M. Teresa Fernández-Abedul,[a] Jorge Pérez-Juste,[b,*] Isabel Pastoriza-Santos,[b] Karen Faulds,[c] Duncan Graham,[c] M. Carmen Blanco-López[a,*]

Establishing a definitive diagnosis of pneumonia using conventional tests is difficult and expensive. Lateral flow immunoassays (LFIAs) are an advantageous point of care (POC) test option, but they have some limitations in terms of detection and quantification. In this work we have developed a lateral flow immunoassay for the ultrasensitive detection of penumolysin employing plasmonic Surface-Enhanced Resonance Raman Scattering (SERRS) tag as labelled probe. The combination of Au@Ag core-shell nanoparticles as plasmonic platform and Rhodamine B Isothiocyanate as Raman reporter has allowed us to fabricate a SERRS tag with high efficiency and reliability. The limit of quantification of the SERRS-based LFIA was 1pg/mL, while the limit of detection was 3.6 pg/mL. This could be a strong foundation for a pneumonia diagnosis test based on pneumolysin detection..

Introduction

Pneumonia is an inflammatory condition of the alveolar spaces of the lungs caused mainly by *Streptococcus pneumoniae*, a pathogenic bacterium which affects two thirds of both adults and children.[1] Establishing a definitive diagnosis of pneumonia is difficult using conventional diagnostic tests. For instance, X-ray isolation of *S. pneumoniae* from blood lacks sensitivity, and other methods such as culture tests are time consuming. Alternatively, invasive tests are rarely performed and, besides they are very expensive.[2]

Nowadays, the most advantageous option is the development of a point-of-care (POC) test, based on antigen detection. These assays are portable, with short analysis time, and they can be used by untrained personnel in any location.[3, 4] Lateral Flow immunoassay (LFIA) is a very successful POC test in which an immunoassay takes place at a membrane. The sample and other reagents move by capillarity forces to a prepared test zone and to a control zone, where the detection antibody is retained giving a visual signal. The results are generally taken within a period of 10 - 20 minutes.

A lateral flow immunoassay for the detection of C-polysaccharide in urine is commercially available and has been approved by the Federal Drug Administration (FDA, USA), as a diagnostic antigenic marker for *S. pneumoniae* (Binax NOW® S. pneumoniae Urinary Anting Test, Binax, Portland, ME, USA).[5-7] This test has a high sensitivity for use in adults,[8, 9] but has the disadvantage of having a low specificity in children, since the latter may result in some cross-reactivity with other carbohydrate antigens.[10, 11] On the contrary, when the detection is based on the pneumolysin protein (PLY), another antigenic marker for *S. pneumoniae*, the cross reaction is supressed.[12]

Unfortunately, the major limitation of these assays is lack of sensitivity and possibility for quantification.[13, 14]Very often they are just used as screening tests, just for qualitative analysis, using colour changes for naked-eye detection, but this is normally insufficient for most of the clinical analytes. To improve their sensitivity and quantification capability, optical reading systems (cameras, scanners or bench top instruments)[15-17] have been used in combination with image analysis software, to take a reading related to the optical density at the test zone. However, these readers lack high precision and sensitivity.

Surface-enhanced Raman scattering (SERS) spectroscopy is an ultrasensitive analytical technique[18-20] that allows the detection of analytes in very low concentration. SERS is based on the plasmon-assisted scattering of analytes on or near metal nanostructures that support localized surface plasmon resonance (LSPR), typically gold or silver. This could lead to an enhancement (up to 10^{11}) of their characteristic ineslastic Raman scattering signal.[21] The direct sensing approach yields both qualitative and quantitative data based on the SERS spectra in presence of the analyte. A further improvement in the sensitivity of Raman scattering spectroscopy arises from the resonance enhancement (surface-enhanced resonance Raman scattering, SERRS) effect that takes place when the excitation wavelength is carefully chosen to overlap with (or be very close to) an electronic transition of the target molecule – this

[a] Departamento de Química Física y Analítica, Universidad de Oviedo, 33006 Oviedo, Spain.
[b] Departamento de Química Física and CINBIO, Universidade de Vigo, 36310 Vigo, Spain.
[c] Centre for Molecular Nanometrology, Department of Pure and Applied Chemistry, WestCHEM, University of Strathclyde, Glasgow G1 1RD, United Kingdom.

Electronic Supplementary Information (ESI) available: Additional TEM images and UV-Vis spectra of Au@Ag NPs, additional characterization of the SERRS tags. See DOI: 10.1039/x0xx00000x

typically occurs in UV-visible region. Thus, both enhancements, from the plasmon resonance (SERS) and target molecular resonance (R) contribute to obtain even greater enhancement factors and therefore to significantly decrease the detection limits and measurement times.[22, 23]

SERS-encoded particles (or SERS tags) are an appealing new class of labeling contrast agents that combine plasmonic metal nanoparticles (NPs) and a Raman reporter molecule.[24] SERS tags produce strong and characteristic Raman signals which can be used for the indirect ultrasensitive detection of a molecule of interest. Also, a further improvement in the sensitivity can be achieved through employing SERRS tags. Additionally, this type of probes presents the multiplexing and quantitative abilities of the SERS technique, showing extraordinary features for bioanalysis.[25] Au and Ag NPs are the most commonly materials employed for the preparation of SERS tags, being silver the material with higher SERS efficiency, from 10-fold to 100-fold times, than those of similar gold nanostructures.[26, 27]

Therefore, the integration of a SERS-encoded nanoparticles within an immunoassay test will lead to an immunoassay with improved sensing capabilities.[28] For instance, different SERS immunoassay platforms for the sensitive detection of protein targets have been proposed based on controlled assembly of SERS-encoded nanoparticles through the sandwiched antibody–antigen interactions.[29-31] Alternatively, the SERS-encoded nanoparticles could be used directly in optical labelling for SERS imaging[25] or the development of SERS-based ELISA analogs with detection sensitivities of two or three orders of magnitude higher than the conventional ELISA.[32-34] Additionally, lateral flow assays or immunochromatographic test strips provide advantages in interference levels, simplicity and rapidity which make us to envision a great potential for ultrasensitive detection when coupled to SERS-encoded nanoparticles.[35, 36] Improvements at the limit of detection have been reported when those particles were AuNP or hollow AuNP. In the present work, we have synthetized a SERRS-tag based on citrate stabilized Au@Ag core-shell NPs, which can be readily encoded with a Raman reporter and subsequently bioconjugated by passive adsorption due to electrostatic and hydrophobic interactions between the protein (anti-pneumolysin antibody, PLY-7) and the metal nanoparticle surface. This is the first time that this core-shell NPs are applied to develop a LFIA coupled to SERRS for the ultrasensitive detection and quantification of pneumolysin, an important biomarker of pneumonia. The antibody functionalized SERRS tags were tested for the detection of pneumolysin in a LFIA by SERRS, thereby analyzing the quantification capabilities and limit of detection related to the conventional colorimetric test and other methods reported in the literature.

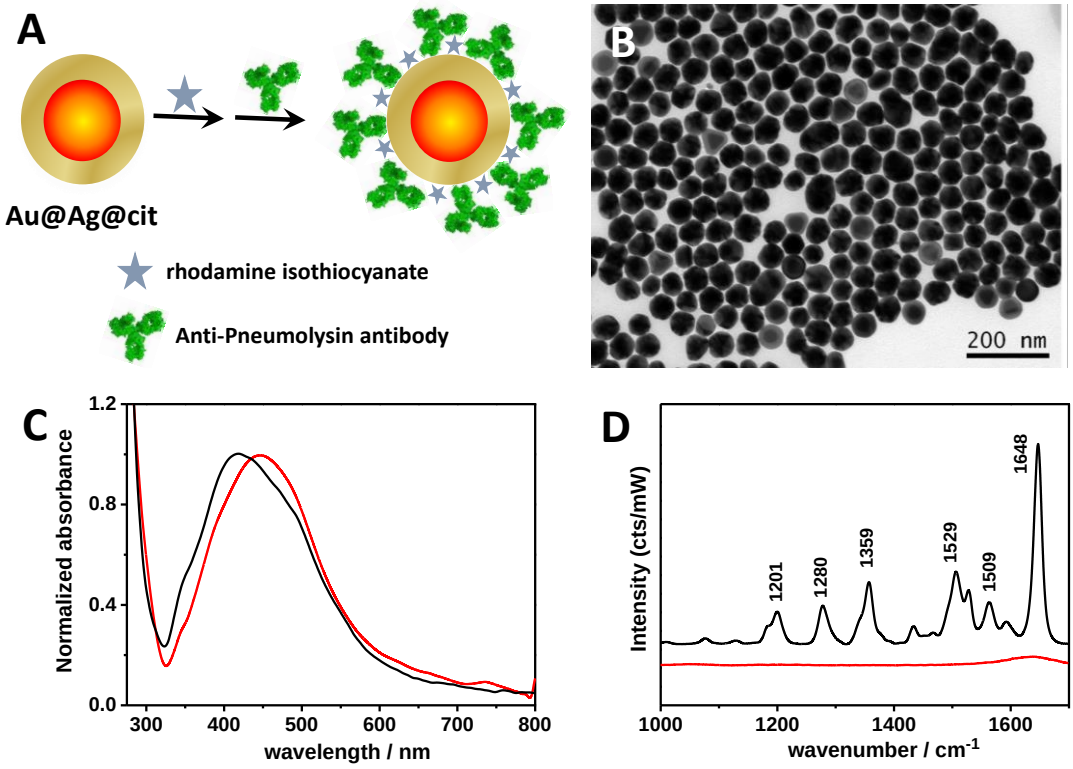

Figure 1. (A) Schematic representation of the fabrication of Au@Ag SERRS tags. (B) Representative TEM image of the Au@Ag tags. (C) Normalized UV-Vis spectra of the as synthetized Au@Ag nanoparticles (black line) and after the Raman encoding and bioconjugation steps (red line). (D) SERRS spectrum of Au@Ag nanoparticles encoded with Rhodamine B isothiocyanate upon excitation with a 532 nm laser line. Acquisition time 1 s. The SERS spectrum of Au@Ag nanoparticles before their encoding (red spectrum) has been included as a blank.

Results and discussion

SERRS encoded Au@Ag nanoparticles.

The fabrication of the SERRS-tags is schematically depicted in **Figure 1A**, and comprised the synthesis of citrate stabilized Au@Ag core-shell nanoparticles, the encoding with a Raman active molecule and the bioconjugation with an antibody. The election of Au@Ag core-shell nanoparticles as SERRS tags could be explained in terms of: i) more effective coupling with the 532 nm excitation laser for Au@Ag NPs (they have larger extinction contribution above 500 nm than pure Ag NPs with similar size),[37] and ii) the higher efficiency of Ag in comparison with Au.

The Au@Ag core-shell nanoparticles were synthesized using a seeded growth strategy[37] based on the stepwise reduction of a silver salt precursor on performed Au nanoparticles of ca. 34 nm in diameter (see experimental section for details). The resulting core-shell structures are very uniform in size and morphology with an average silver shell of 12 nm (**Figures 1B and S1 in ESI**). The analysis of their optical properties shows a localized surface plasmon band (LSPR) centered at 420 nm. Subsequently, encoding with the Raman reporter Rhodamine B isothiocyanate was carried out by simply adding the dye to a colloidal dispersion of Au@Ag NPs. The sulphur-containing isothiocyanate group of the dye ensured its chemical binding to metal surface. Excess dye molecules were removed by a centrifugation-redispersion cycle. The surface modification of the particles leads to decrease in the average ζ-potential from -45.1 mV to -38.9 mV. Finally, the Ag surface was bioconjugated with anti-pneumolysin antibody (PLY-7) via adsorption induced by electrostatic and hydrophobic interactions. After the Rhodamine B encoding and PLY-7 bioconjugation steps (PLY-7-Au@Ag SERRS tags) the extinction spectrum of the Au@Ag colloids was red-shifted 25 nm (**Figure 1C)** from 420 nm to 445 nm. This behavior can be attributed to an increase in the local refractive index of the surrounding medium mediated by the protein and dye adsorption.

The SERRS efficiency of the encoded Au@Ag NPs was analysed at 532 nm, laser excitation in resonance with the absorption band of Rhodamine B isothiocyanate (Figure S2 in the SI). As shown in Figure 1D the characteristic SERRS signals of Rhodamine B were recorded from the labeled nanoparticles:[38] 1647 cm^{-1}, 1562 cm^{-1}, 1529 cm^{-1}, 1509 cm^{-1} and 1359 cm^{-1} (aromatic C–C stretching), 1280 cm^{-1} (C-C bridge-bands stretching) and 1201 cm^{-1} (aromatic C-H bending). No SERS signals were recorded from Au@Ag nanoparticles before their encoding. The SERRS efficiency and reproducibility of the Au@Ag tags were analysed by plotting the intensity of the most intense SERRS signal of Rhodamine, 1647 cm^{-1}, as a function of particle concentration (see Figure S2 in ESI). The plot showed linear correlation with small standard deviations over the range (0.10-10.0 pM), being 0.10 pM the lowest detectable Au@Ag nanoparticle concentration.

Immunoassay design and SERRS detection at the strips

The principle of the SERRS-based LFA strip is based on a sandwich immunoassay. The nitrocellulose membrane was initially washed by immersion in a solution of running buffer during 1h. After that, the strips were dried for 1h at room temperature to remove any commercial additive that could interfere with the measurement. Subsequently, mouse monoclonal anti-PLY antibody, PLY-4 (capture antibody) and anti-mouse IgG antibody were immobilized on the test and control lines of the LFA strip, respectively. The sample solution with the antigen, antibody-conjugated PLY-7-Au@Ag rhodamine encoded SERRS tags, and the running buffer was added into the microtube and the sample was allowed to run for 10 min in a dipstick format. Then the sample solution migrates by capillarity, being captured with the anti-PLY-4 previously immobilized on the strip test line (see **Figure 2A** and experimental section for details). The excess of the PLY-7-Au@Ag SERRS tags continues migrating along the membrane where they are captured by the anti-mouse IgG antibody immobilized on the control line. The accumulation of Au@Ag NPs in either the test or control lines produces a characteristic dark/brown band in the test zone, with a colour

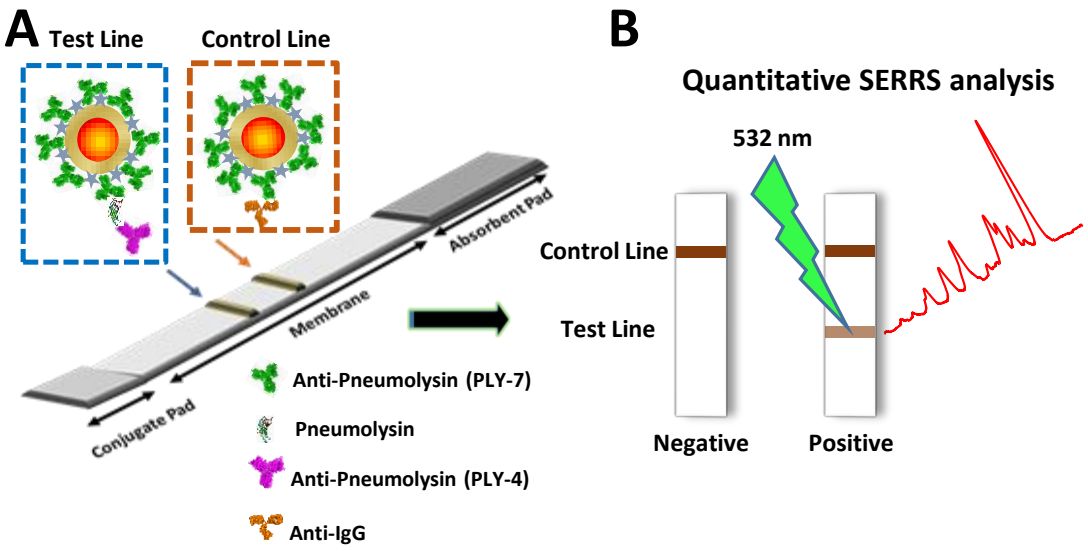

Figure 2. (A) Schematic Illustration of the SERRS-based LFIA strip. (B) Qualitative analysis in the strip, where only one brown line is observed in the control zone in the absence of pneumolysin (Negative) and two lines appear in presence of the pneumolysin (positive). The SERRS characterization of the test line allows a quantitative analysis.

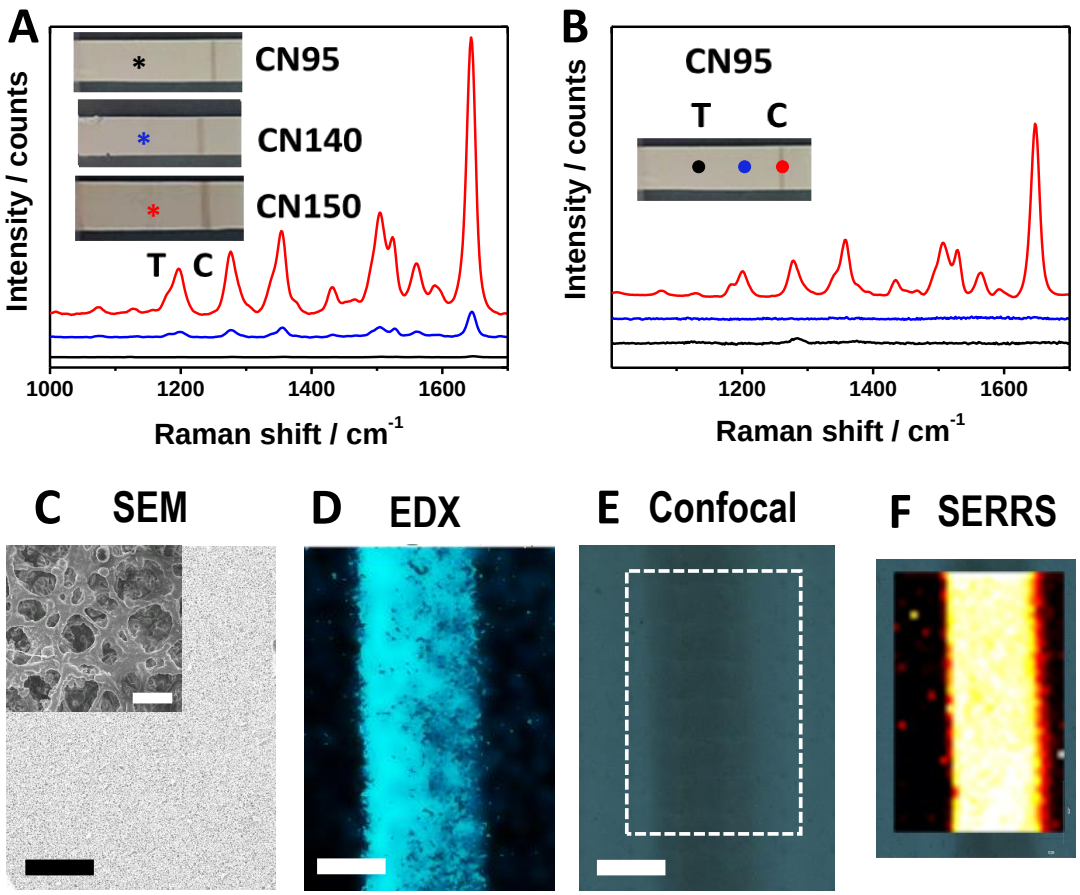

Figure 3. (A) SERRS spectra measured at the test line for the three different nitrocellulose membranes employed in the LFIA. The inset shows a photograph of the membranes and the coloured dots indicate the corresponding spectrum. (B) SERRS spectra measured at three different points on the CN95 membrane as indicated by the coloured dots. (C) Representative SEM image of the LFIA strip along the control line (the inset shows a high magnification SEM image of the membrane surface, the scale bar represents 10 µm) and the corresponding EDX maps performed using the Ag L_α line (C). (D) Confocal image of the control line. (E) SERRS map of the region highlighted in D collected from the 1647 cm^{-1} signal. Scale bars represent 500 µm.

intensity that is related to the concentration of analyte. Two darks/browns bands appear in the presence of the pneumolysin indicating the positive test (**Figure 2B**), whereas only a dark/brown band is observed in the control zone when no pneumolysin is present (a negative test). This line band in the control zone will act as a verification of the good behavior of the LFIA strip. In order to record an instrumental analytical signal and check the validity of the immunoassay, the test and control lines were analysed in the Raman spectrophotometer under the 532 nm laser line excitation (see experimental section for details). The characteristic spectrum of the RBITC dye could be monitored. The peak at 1647 cm^{-1} was taken as reference for the measurements.

Optimization of the SERRS-LFI Assay parameters

Different parameters have been evaluated to optimise the assay, in order to provide a good transport of the SERRS tag along the membrane. Particularly, we have evaluated the influence of the nitrocellulose membrane and the running buffer.

The nitrocellulose membrane used as strip material is probably the most important part of the test system.[4] Various types of membranes with a different capillary speed rate are available. For this work, nitrocellulose UniSart CN95, CN140 and CN150 membranes with different pore sizes and capillary speed were tested (see **Table S1** in the ESI). The pore size and the material are important for both the transport of the label, and the speed at which the conjugate complex is transported through the membrane allowing optimal reaction time.[39] To check the suitability of the different membranes for the LFIA a qualitative SERRS evaluation of the test line at a negative control was carried out. These experiments allowed us not only to check the suitability of the membranes but also to discard cross-reaction effects among detection and capture antibodies. **Figure 3** shows photographs of three different LFIA strips after performing the negative text. In the absence of the target antigen, the accumulation of Au@Ag SERRS tags on the control line led to a colour change easily visible by the naked eye, while no color change was observed in the test line. However, the SERRS analysis of the three test lines revealed the characteristic Raman signal of the SERRS encoded nanoparticles for the nitrocellulose membranes with the lower capillary speed (CN140 and CN150, see **Figure 3**), confirming a higher non-specific signal, while no signals were detected in the membrane with the fastest capillary speed (CN95, see **Figure 3**).

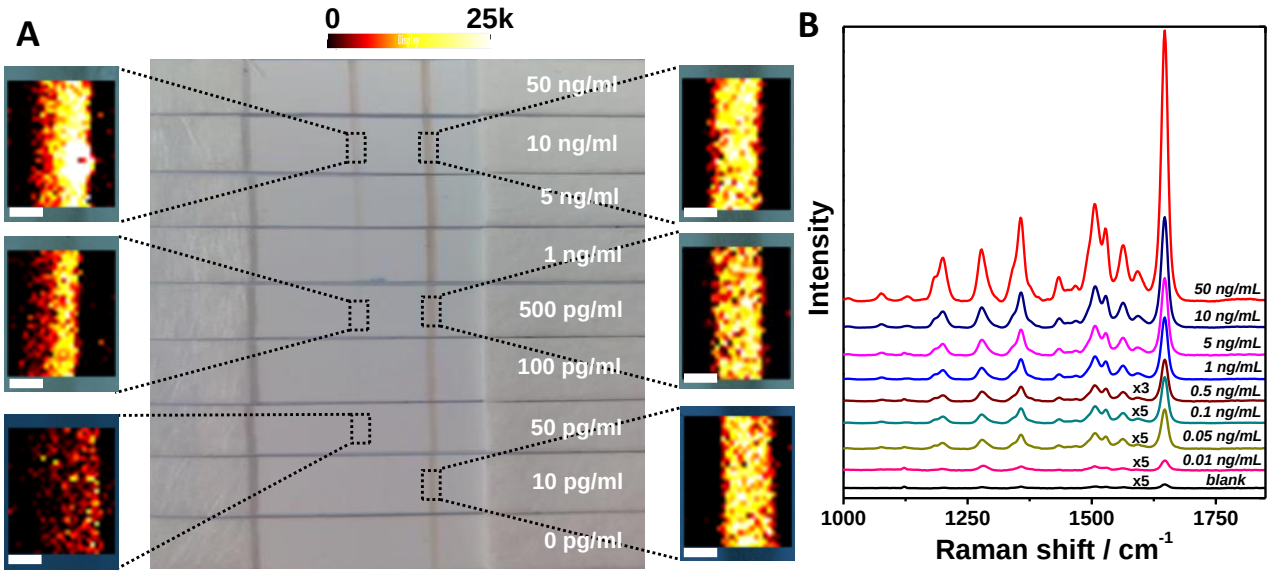

Figure 4. (A) Photographs of different LFIA strips in the presence of different pneumolysin concentrations as indicated. SERRS mappings using the 1647 cm^{-1} band. Scale bars represent 500 µm. All SERRS measurements were carried out with a 532 nm laser line, 10x objective, 0.4 mW laser power, acquisition time 1s, step 50 µm x 50 µm, 1300 x 1550 µm, 806 points. (B) Average SERRS spectra from 50 random points measured in the test lines.

To confirm whether or not the SERRS detection of the bioconjugate is efficient, and the sandwich is only bound on the test line, and not unspecifically at the membrane, different spectra were recorded at the test and control lines, and also at different positions of the CN95membrane. The presence of the characteristic SERRS bands solely at the control line demonstrated the specificity of the test and the absence of cross-reaction effects among detection and capture antibodies (**see Figure 3**). Additionally, we have performed SEM characterization of the membrane. Figure 3C shows a representative SEM image of the membrane surface where the Au@Ag tags could not be distinguished. Therefore, in order to analyse the spatial distribution of the SERRS tags on the membranes we performed elemental mapping through energy-dispersive X-ray spectroscopy (EDX). Figure 3D shows the EDX elemental map showing the distribution of Ag ($L_{\alpha 1}$ line), and therefore of Au@Ag NPs, in a line of ca. 1mm width. These results are in agreement with those obtained by SERRS mapping of the control line. Figures 3E and 3F show a confocal image of the control line and the corresponding SERRS mapping recorded at 1647 cm^{-1}. All together demonstrates that the presence of the SERRS encoded nanoparticles is solely on the control line, and validating the efficient SERRS detection of the bioconjugate.

The running buffer solution could also strongly affect the performance of the sensor and the immunoassay. Three different types of running buffer solutions were tested namely; phosphate buffered saline (PBS), borate buffered saline (BBS) and HEPES ((4-(2-hydroxyethyl)-1-piperazineethanesulfonic acid). PBS was selected as the running buffer since the BBS and HEPES buffers could compromise the stability of the bioconjugate. Besides, the amount of BSA and surfactant (Tween 20) in the running buffer can also influence the sensitivity of the visual and instrumental signal. Thus, a BSA concentration of 1.0% was enough for block the membrane without affecting the line signal, and 0.05% Tween 20 for a better performance of the assay.

Quantitative analysis of pneumolysin using the SERRS-based lateral flow assay

After the optimization of the experimental conditions, quantitative analysis of pneumolysin with SERRS-based LFIA was performed as a proof of concept. Additionally, the optical response of the Au@Ag nanoparticles in the visible region of the spectrum (Figure 1C) allow us to performed the pneumolysin detection by means of point POC-LFIA based on optical density. For this purpose, different concentrations of the pneumolysin were examined. Figure 4A shows photographs of the LFIA strips in the presence of different concentrations of Pneumolysin from 10 pg/mL to 50 ng/mL. The presence of target antigens was confirmed through a colour change in the test line. It can be observed that the brown colour becomes darker for more sandwich conjugate formed. Consequently, the presence of target antigens can be identified by the naked eye, as in a conventional LFIA strip. A dark/brown band was observed in the test zone down to a concentration of pneumolysin of 1 ng/mL. Additionally, the SERRS-based LFIA strips allowed a quantitative evaluation of target antigens by measuring SERRS signals characteristics of the Au@Ag encoded tags. For the SERRS quantitative analysis of the strips, SERRS signal was recording on the test line, Figure 3 shows SERRS mapping images obtained over an extended area of 1300 µm x 1550 µm (806 pixel points with a 50 µm x 50 µm step) in both, the test and the control lines. The control line shows an excellent uniform SERRS intensity over the whole line in all cases, that is, regardless of the pneumolysin concentration (Figure 4). The test line also shows a uniform SERRS signal but decreases with decreasing the pneumolysin concentration from 50 ng/mL to 10 pg/mL. It should be noted that the SERRS signal intensity is quite homogenous especially at higher pneumolysin

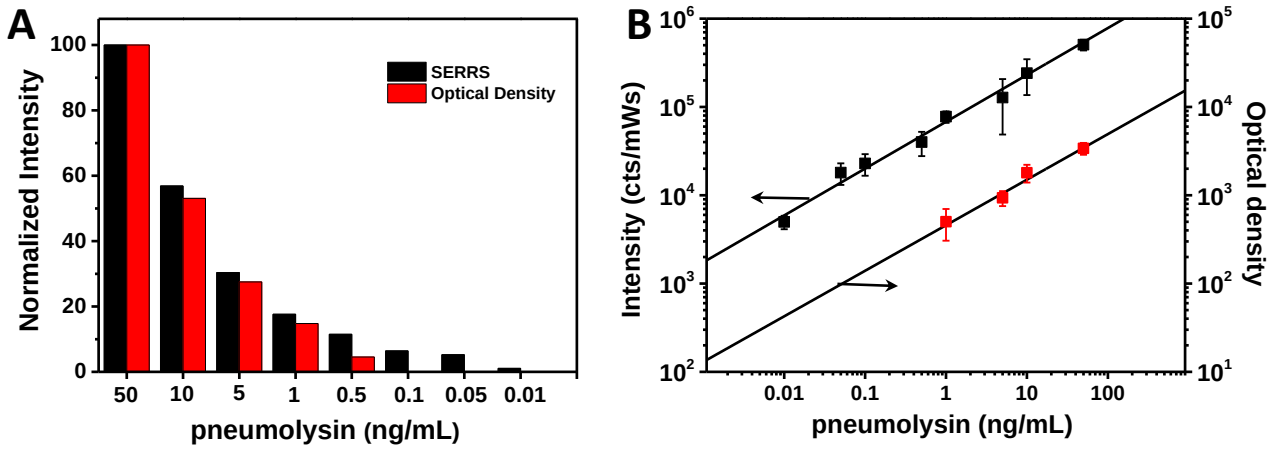

Figure 5.(A) Evaluation of the results obtained for different pneumolysin concentrations using the point of case-based LFIA(red columns) and SERRS-based LFIA (black columns) through optical density and SERRS measurements, respectively. (B)Quantification range for pneumolysin employing the POC-LFIA strip (red squares) or the SERRS-based LFIA strip (blacksquares).

concentrations. In order to construct a calibration curve for quantitative calibration up to 50 points from three independent experiments were averaged for each pneumolysin concentration. The small intensity deviation indicate that the SERRS signals obtained present a good analytical reproducibility. Figure 4B shows the average SERRS spectra measured for each pneumolysin concentration.

We have compared the sensitivity of this SERRS based LFIA with the value that could be achieved based on the optical density reading of the test line. In order to get this measurement, the images taken with the camera of a smartphone on freshly run strips were processed with the ImageJ 1.49v software (see experimental section). Figure 5 shows a comparison of the results obtained for the pneumolysin detection with the both systems. In the SERRS-based assay the intensity of the Raman band at 1647 cm^{-1} was selected for the quantitative evaluation. It can be clearly seen that a more sensitive quantification of pneumolysin was achieved with the SERRS-based LFIA. The limit of detection (LOD) of the SERRS-based LFIA, calculated as the concentration corresponding to 3 times the standard deviation of the blank, was 1 pg/mL (see Table S3 in the ESI), whereas with the analysis of the images there was not detection below 1 ng/mL. Some of the lowest LOD values reported in the literature for pneumolysin detection with the same immunological system are 0.6 ng/ml (electrochemical immunosensor)[40] and 5.5 pg/ml (by a chemiluminescent immunoassay).[41] Therefore, SERRS-LFIA developed in this work improved significantly the LOD for the determination of this biomarker.

Conclusions

In summary, we have demonstrated that Au@Ag SERRS tags can be used as labelled probes in a lateral flow immunoassay for the ultrasensitive detection of pneumolysin. The principle of the SERRS-based LFA strip is based on a sandwich immunoassay, being the RBITC encoded Au@Ag tags the SERRS detection probes. The Au@Ag NPs allowed the detection and quantification through both, SERRS-based LFIA and optical density readings. The limit of detection for the SERRS-based LFIA strip was estimated to be 3.6 pg/ml. The coupling of a SERRS-based sensor within a lateral flow immunoassay strip will boost its sensitivity and quantitative capabilities, showing a great potential for the qualitative and quantitative detection of analytes in biomedical, food and environmental analysis.

Experimental

Materials

Tetrachloroauric acid ($HAuCl_4 \cdot 3H2O$), L-ascorbic acid (AA, >99% pure), trisodium citrate dihydrate, silver nitrate ($AgNO_3$, >99% pure), bovine serum albumin (BSA), Rhodamine B Isothiocyanate (RBITC), phosphate-buffered saline (BPS), Tween-20, boric acid, 4-(2-hydroxyethyl)-1-piperazineethanesulfonic acid (HEPES) and anti-mouse IgG was purchased from Sigma-Aldrich (Spain). Mouse monoclonal anti-PLY antibodies PLY-4 (capture antibody) and PLY-7 (detection antibody) were produced by Core Service of the University of Oviedo (Oviedo, Spain).

Nitrocellulose (NC) membranes (UniSart CN95, CN140, CN150) were purchased from Sartorius (Spain). Glass fiber sample pads (GFCP001000) and absorbent pads from Millipore, backing cards (KN-V1080, Kenoshatapes, Netherlands).

Instrumentation

IsoFlow reagent dispensing system (Imagene Technology,USA) was used to dispense the detection line. A guillotine Fellowes Gamma (Spain) was used to cut the strips.

SERRS experiments were conducted with a Renishaw InVia Reflex confocal system. The spectrograph used a high-resolution grating (1800 grooves mm^{-1}) with additional band-pass filter optics, a confocal microscope, and a 2D-CCD camera. SERRS characterization of doped nanoparticles was done using a Snowy range instrument (excitation of 532 nm and 50mW of maximum power) to measure in

liquid state. SERRS images were obtained using a point-mapping method with a 50× objective (N.A. 0.40), which provided a spatial resolution of about 2.6 μm^2. It created a spectral image by measuring the SERRS spectrum of each pixel of the image, one at a time. The SERRS images of each well were decoded using the characteristic peak intensities of the Raman reporter molecule (RBITC, 1647 cm^{-1}) using WiRE software V 4.1 (Renishaw, UK). SERRS spectra were analyzed using Grams software (Thermo Scientific, USA). The limit of detection (LOD) of the SERRS-based LFIA is calculated as the concentration corresponding to 3 times the standard deviation of the blank.

Optical characterization was carried using a Cary 300 UV-Vis spectrophotometer (Varian, Salt Lake City, UT, USA). TEM images were acquired with a JEOL JEM 1010 TEM operating at an acceleration voltage of 100 kV. SEM images were obtained using a JEOL JSM-6700F FEG scanning electron microscope operating at an acceleration voltage of 10.0 kV.

The optical density of the capture image from the signal monitoring window was digitized using ImageJ 1.49v software.

Synthesis of Au NPs. Citrate-stabilized Au NPs were prepared by the kinetically controlled seeded growth method reported by Bastus et al.[27] Briefly, 150 mL of 2.2 mM trisodium citrate in Milli-Q water was heated to boiling while being vigorously stirred. After 15 min, 1 mL of 25 mM $HAuCl_4$ was injected into the boiling reaction mixture, and after 10 min, the reaction mixture was cooled to 90 °C. Subsequently, 1 mL of a 25 mM $HAuCl_4$ aqueous solution was injected into the reaction mixture, and after 30 min, 1 mL of the same solution was injected again. After additional 30 min, 55 mL of the sample was extracted and 53 mL of water and 2.2 mL of 60 mM sodium citrate was added. The final solution was then used as a seed solution, and the process was repeated (but with just two injections of the $HAuCl_4$ aqueous solution) again three times to yield Au NPs with an average diameter of 34.2 ± 5.0 nm (see Figure S1 in ESI).

Synthesis of Au@Ag Core-Shell NPs. Citrate-stabilized Au@Ag NPs were prepared accordingly to the procedure previously reported by Samal et al. with some modifications.[24] Briefly, 60 µL of AA (200 mM) and 15 µL of $AgNO_3$ (200 mM) were added to a beaker containing 10 mL of as-prepared Au NPs seeds (~34 nm) at room temperature. The reaction was continued for 30 min while the mixture was slowly stirred. Then, 60 µL of AA (200 mM) and 15 µL of $AgNO_3$ (200 mM) were added (second cycle). The gradual increase in Ag shell thickness was monitored by UV–visible spectroscopy. After ten additions, the resulting particles were centrifuged at 301 g for 20 min and redispersed in 10 mL of water. The final Au@Ag core-shell NPs was 58.3 ± 5.7 nm (see Figure S1 in ESI). The average ζ-potential of the encoded particles was -45.1 mV. The Au@Ag nanoparticles concentration was estimated from the concentration of the gold NPs used as seeds and assuming that no free nucleation occurs during the silver overgrowth process (see ref. 37).

Fabrication of SERRS encoded Au@Ag NPs. The codification with the Raman probe was carried out by simply adding dropwise 10 µL of a solution of RBTIC ($9.6x10^{-5}$ M) in methanol under gentle stirring to 1 mL of as prepared Au@Ag NPs in water. Stirring was continued for 1 hour and then the mixture was centrifuged at 301 g for 20 min to remove RBITC excess and redispersed in 1 mL of water. The average ζ-potential of the encoded particles was -38.9 mV.

Conjugation of SERRS tags with Anti PLY-7 antibody. Typically, 500 µL of Au@Ag NPs were centrifuged at 301 g for 20 min at 4 °C. The pellet was resuspended in 500 µL of H_3BO_3 pH 7.6 with 20 µg/mL of the detection antibody Anti PLY-7. After one hour of incubation and mixing at room temperature, the sample was centrifuged and the pellet resuspended in 500 µL of blocking and storage buffer (boric acid + 1% BSA). The sample was then centrifuged once again and resuspended in 250 µL of H_3BO_3 pH 7.6 (storage buffer) and kept at 4 °C. The different steps of the conjugation were monitored by UV–visible spectroscopy (Figure 1).

Fabrication of the LFIA strips. To fabricate the strip, the nitrocellulose (NC) membrane was attached to a plastic backing card. The test and control zone of the strip were prepared by dispensing 1 mg/mL mouse monoclonal PLY-4 anti-pneumolysin and anti-IgG respectively with the IsoFlow dispenser onto NC membrane at a dispensing rate of 0.100 µL/mm. The strips were dried at 37 °C for 30 min. The conjugate and absorbent pads, were attached to both ends of the membrane on the backing card with an overlap between them of around 2.5 mm approximately. The complete strip was cut into individual 5 mm strips.

For the optical density measurements, photographs of the freshly run strips were taken with smartphone camera (13 MP) and they were analysed by means of the ImageJ 1.49v software. The brightness of the surroundings was controlled and a proper calibration of the color intensity at exactly the same conditions was carried out. The color of test lines displayed clear gradient according with the concentration of pneumolysin.

Acknowledgements

This work was supported by the Ministerio de Economía y Competitividad (MINECO, Spain), under the Grant CTQ2013-47396-R, CTQ2014-58826-R, MAT2013-45168-R and MAT2016-77809-R. This study was also financed by the Consejería de Economía y Empleo del Principado de Asturias (Plan de Ciencia, Tecnología e Innovación 2013-2017), under the Grant GRUPIN14-022 and FC-15-GRUPIN14-021. V.M.-G. acknowledges FPU scholarship from the Spanish MINECO. A.G acknowledges EPSRC (Engineering and Physical Sciences Research Council.

Notes and references

1 M. Díaz-González, M. B. González-García and A. Costa-García, *Sensor Actuat. B-Chem.*, 2006, **113**, 1005-1011.
2 A. Ruiz-González, M. Falguera, A. Nogués and M. Rubio-Caballero, *Am. J. Med.*, 1999, **106**, 385-390.
3 P. B. Luppa, C. Muller, A. Schlichtiger and H. Schlebusch, *Trac-Trend Anal Chem*, 2011, **30**, 887-898.
4 G. A. Posthuma-Trumpie, J. Korf and A. van Amerongen, *Anal. Bioanal. Chem.*, 2009, **393**, 569-582.

5 M. D. García-Suárez, M. D. Cima-Cabal, R. Villaverde, E. Espinosa, M. Falguera, J. R. de Los Toyos, F. Vázquez and F. J. Méndez, *J. Clin.Microbiol.*, 2007, **45**, 3549-3554.
6 J. Domínguez, N. Gali, S. Blanco, P. Pedroso, C. Prat, L. Matas and V. Ausina, *Chest*, 2001, **119**, 243-249.
7 D. R. Murdoch, R. T. R. Laing, G. D. Mills, N. C. Karalus, G. I. Town, S. Mirrett and L. B. Reller, *J. Clin.Microbiol.*, 2001, **39**, 3495-3498.
8 F. Andreo, J. Domínguez, J. Ruiz, S. Blanco, E. Arellano, C. Prat, J. Morera and V. Ausina, *Resp. Med.*, 2006, **100**, 884-891.
9 M. L. Briones, J. Blanquer, D. Ferrando, M. L. Blasco, C. Gimeno and J. Marín, *Clin. Vaccine. Immunol.*, 2006, **13**, 1092-1097.
10 J. Domínguez, S. Blanco, C. Rodrigo, M. Azuara, N. Gali, A. Mainou, A. Esteve, A. Castellvi, C. Prat, L. Matas and V. Ausina, *J. Clin.Microbiol.*, 2003, **41**, 2161-2163.
11 S. F. Dowell, R. L. Garman, G. Liu, O. S. Levine and Y. H. Yang, *Clin. Infect. Dis.*, 2001, **32**, 824-825.
12 K. P. Klugman, S. A. Madhi and W. C. Albrich, *Clin. Infect. Dis.*, 2008, **47**, S202-S206.
13 Y. Q. He, X. B. Zhang, S. Q. Zhang, M. K. L. Kris, F. C. Man, A. N. Kawde and G. D. Liu, *Biosens. Bioelectron.*, 2012, **34**, 37-43.
14 H. A. Joung, Y. K. Oh and M. G. Kim, *Biosens. Bioelectron.*, 2014, **53**, 330-335.
15. C. Y. Liu, Q. J. Jia, C. H. Yang, R. R. Qiao, L. H. Jing, L. B. Wang, C. L. Xu and M. Y. Gao, *Anal. Chem.*, 2011, **83**, 6778-6784.
16. R. C. Murdock, L. Shen, D. K. Griffin, N. Kelley-Loughnane, I. Papautsky and J. A. Hagen, *Anal. Chem.*, 2013, **85**, 11634-11642.
17. M. Oliveira-Rodríguez, E. Serrano-Pertierra, A. Costa García, S. López-Martín, M. Yañez-Mo, E. Cernuda-Morollón and M. C. Blanco-López, *Biosens. Bioelectron.*, 2017, **87**, 38-45.
18. M. Moskovits, *J. Raman Spectrosc.*, 2005, **36**, 485-496.
19. P. L. Stiles, J. A. Dieringer, N. C. Shah and R. R. Van Duyne, *Annu. Rev. Anal. Chem.*, 2008, **1**, 601-626.
20. S. Schlucker, *Angew. Chem., Int. Ed.*, 2014, **53**, 4756-4795.
21. Y. Fang, N. H. Seong and D. D. Dlott, *Science*, 2008, **321**, 388-392.
22. E. C. Le Ru and P. G. Etchegoin, *Principles of Surface-Enhanced Raman Spectroscopy*, Elsevier, New York, NY, USA, 2009.
23. G. McNay, D. Eustace, W. E. Smith, K. Faulds and D. Graham, *Appl. Spectrosc.*, 2011, **65**, 825-837.
24. Y. Q. Wang, B. Yan and L. X. Chen, *Chem. Rev.*, 2013, **113**, 1391-1428.
25. G. Bodelon, V. Montes-Garcia, C. Fernandez-Lopez, I. Pastoriza-Santos, J. Perez-Juste and L. M. Liz-Marzan, *Small*, 2015, **11**, 4149-4157.
26. M. F. Cardinal, B. Rodriguez-Gonzalez, R. A. Alvarez-Puebla, J. Perez-Juste and L. M. Liz-Marzan, *J. Phys. Chem. C*, 2010, **114**, 10417-10423.
27. F. J. G. de Abajo, *Rev. Mod. Phys.*, 2007, **79**, 1267-1290.
28. X. Fu, L. Chen and J. Choo, *Anal. Chem.*, doi: 10.1021/acs.analchem.1026b02251.
29. Y. Wang, C. H. Zhang, L. J. Tang and J. H. Jiang, *Anal. Chem.*, 2012, **84**, 8602-8606.
30. A. Q. Yang, D. Wang, X. Wang, Y. Han, X. B. Ke, H. J. Wang, X. Zhou and L. Ren, *RSC Adv.*, 2015, **5**, 38354-38360.
31. X. L. Wu, X. Chen, F. L. Gan, W. Ma, L. G. Xu, H. Kuang, A. K. Li and C. L. Xu, *Biosens. Bioelectron.*, 2016, **75**, 55-58.
32. J. Ni, R. J. Lipert, G. B. Dawson and M. D. Porter, *Anal. Chem.*, 1999, **71**, 4903-4908.
33. J. H. Ko, S. Lee, E. K. Lee, S. I. Chang, L. X. Chen, S. Y. Yoon and J. Choo, *Phys. Chem. Chem. Phys.*, 2013, **15**, 5379-5385.
34. Y. L. Wang, M. Salehi, M. Schutz and S. Schlucker, *Chem. Commun.*, 2014, **50**, 2711-2714.
35. X. Fu, Z. Cheng, J. Yu, P. Choo, L. Chen and J. Choo, *Biosens. Bioelectron.*, 2016, **78**, 530-537.
36. J. Hwang, S. Lee and J. Choo, *Nanoscale*, 2016, **8**, 11418-11425.
37. A. K. Samal, L. Polavarapu, S. Rodal-Cedeira, L. M. Liz-Marzan, J. Perez-Juste and I. Pastoriza-Santos, *Langmuir*, 2013, **29**, 15076-15082.
38. P. Hildebrandt and M. Stockburger, *J. Phys. Chem.*, 1984, **88**, 5935-5944.
39. K. Henderson and J. Stewart, *J. Immunol. Methods*, 2002, **270**, 77-84.
40. P. Fanjul-Bolado, M. B. Gonzalez-Garcia and A. Costa-Garcia, *Talanta*, 2004, **64**, 452-457.
41. M. D. Cima-Cabal, F. J. Mendez, F. Vazquez, M. D. Garcia-Suarez and J. R. de los Toyos, *J. Immunoassay Immunochem.*, 2001, **22**, 99-112.
42. N. G. Bastus, J. Comenge and V. Puntes, *Langmuir*, 2011, **27**, 11098-11105.